Heritage Science

RESEARCH

Open Access

A non-destructive analytical study of cultural heritage object from Late Antiquity: gold framework and gemstone inlays

Radek Hanus[1], Kamil Sobek[2*], Kamil Souček[3], Lubomír Staš[3], Lucie Georgiou[3] and Alena Selucká[4]

Abstract

Recently found historical jewellery (Czech Republic) was subjected to detailed analyses to determine the gem inlays and the gold framework in which they are embedded. Such find fits into European jewellery archaeological artefacts containing similar stones from around the fifth century CE. The gemstones were analysed with optical microscopy and Raman micro-spectroscopy to determine their mineralogical characteristics and to find out typical structural-chemical differences based on which their provenance can be found. The results of this measurement discovered two main types of minerals from the garnet group, almandine and pyrope, where pyropes have been identified as Bohemian garnets thanks to the typical photoluminescence (PL) of chromium and vanadium impurities. The craftsmanship and processing of the goldsmith work were studied using X-ray computed tomography. Such a technique is an excellent contribution for detecting and visualising the internal parts hidden behind the placement of the stones. For this reason, 3D visualisation was used to describe and better understand all preserved parts. According to this object's very high cultural and historical value, the chosen methods are suitable for non-destructive study while proving to be essential to deepen our knowledge in archaeometric investigations focused on jewellery from Late Antiquity (with possible application to the jewellery from other periods). Based on the findings presented in this study, it is one of the world's oldest documented items using Bohemian garnets in jewellery. These findings underscore the tremendous economic and political importance of Bohemian garnet mineral resources altogether, with a second completely different type of garnet believed to have originated in distant India or Sri Lanka that was used in jewellery across Europe in Late Antiquity.

Keywords Gemstones, Gold, Micro-Raman spectroscopy, X-ray computed tomography, Late Antique

Introduction

In 2020, during archaeological reconnaissance of the terrain near the locality of Mšec village in the Rakovník region (Central Bohemia—Czech Republic—Central Europe), a hoard of objects made of gold and decorated with gemstones was discovered using a metal detector. The entire set of deposited items consisted of four richly decorated pieces (primarily a catch plate, as well as the frame and tongue of a belt buckle and a ring—Figs. 1 and 2) along with several small fragments that were found on an old trade route, which remains virtually unchanged on many newer maps and still exists today. Based on the identification of the inlaid gemstones and method

*Correspondence:
Kamil Sobek
sobekk@mail.muni.cz
[1] Gemmological Laboratory, Prague, Czech Republic
[2] Department of Geological Sciences, Masaryk University, Faculty of Science, Kotlářská 267/2, 611 37 Brno, Czech Republic
[3] Institute of Geonics, Czech Academy of Sciences, Studentská 1768/9, 708 00 Ostrava-Poruba, Czech Republic
[4] Methodological Centre for Conservation–Technical Museum in Brno, Purkyňova 105, 612 00 Brno, Czech Republic

Fig. 1 Photo of the gold catch plate from a fifth century belt, richly decorated with precious red stones and bluish-green glass inlays. The catch plate is partially damaged. (Photo by M. Frouz)

of manufacturing, all items described in this paper were dated identically by archaeologists from the Rakovník Museum (K. Blažková and J. Bezáková) and the Institute of Archaeology, Faculty of Arts, Charles University (J. Jiřík) to the Late Antique Period, i.e., the fifth century CE on the territory of today's Czech Republic [1–3].

Various red-colour garnets were the dominant gemstones used for jewellery made using the "cloisonné" technique during the Late Antique to Early Middle Ages (4th to eighth century CE) [4–6]. Due to the relatively significant number of finds from this period, there is an extensive collection of analytical/archaeometric data published by various authors using similar or different research methods, such as Particle Induced X-ray Spectroscopy (PIXE), Scanning Electron Microscopy with Energy Dispersive Spectroscopy (SEM–EDS), and electron probe microanalyser (EPMA) [7–10]. From their research, it is evident that we can to some extent observe the individual technological, geological, and socio-geographical aspects of the time, and the obtained data can allow us to explore possible ancient trade routes and material sources [11, 12]. For this investigation, it is essential to focus on the characteristic features of these gemstones, such as the presence of fundamental main or trace elements and inclusions [13], which may serve as a fingerprint to distinguish individual minerals from one another [14].

In terms of the garnets' geological origin and deposition, their distinctive characteristics stem from diverse metamorphic rocks of varying ages. The transition from amphibolite to granulite facies rocks, which include diverse types of schists, gneiss, and amphibolites, formed almandines and pyropes with various chemical compositions. For this reason, it is assumed that these stones could have originated in India, as they fit the geological description and findings of gem garnets from Indian deposits [15–17]. Alluvial deposits derived from the Precambrian metamorphic rocks that make up the island of Sri Lanka, such as granulites, gneiss, schists, and quartzite, frequently include developed jewellery-quality crystals [18]. The chemical diversity of the almandine-pyrope garnets found in the jewellery may indicate multiple sources from the Far East, as this type of stone also matches the observation related to Sri Lanka's diverse geology. Most high-quality pyrope deposits are found in Bohemia. Although the minerals are formed in peridotites, pyrope deposits here are primarily found in alluvial plains south of the Bohemian Massif [19]. With some of the other possible deposits, places of occurrence in Portugal or East Africa can be assumed; however, due to the different chemistry, the use of these gems is less likely. Many of the deposits are still actively yielding gemstones [9, 19, 20].

A very suitable method for measuring these characteristic features of garnets is Raman spectroscopy.

Fig. 2 A series of photos of other items, such as a ring and the frame and tongue of a belt buckle found in the deposition. (Photo by M. Frouz)

Because this method is not only non-destructive but also relatively fast and accurate, it is the perfect tool for studying archaeological objects [21]. Raman spectroscopy can detect tiny changes inside the garnet crystallographic lattice linked to the chemistry of the individual members of these solid solutions. Thanks to this substitution mechanism, numerous types of Si–O vibrations can be observed, allowing us to determine specific Raman spectra for each garnet end member [22, 23]. In addition, inclusions can also be studied and subsequently used as a characteristic feature to improve identification. Each type of garnet will contain different inclusions, as they represent the different environments of formation and origin [7, 9, 10, 16].

Industrial X-ray computational micro-tomography was another method used to study the gold parts of the catch plate of the buckle. As of late, this method has been used more frequently to research, analyse, and non-destructively study the internal construction of examined objects in engineering, geosciences, museology, biology, or archaeology [24–26]. Such X-ray computed tomography data are often used for 3D printing, which can also be employed in reconstructing historical artefacts using 3D printers [27]. The industrial X-ray computed tomography (CT) method enables non-destructive detailed imaging of the examined object in 3D or using suitably oriented 2D tomographic sections.

Materials and methods

Sample description

The subject of the study is a catch plate of the belt buckle made of gold with dimensions 6.3 × 4.2 cm and 1 cm in height (Fig. 1). The sample is decorated with red and green inlays (The term "stone, gemstone or inlay" refers only to the non-metallic part of the jewellery, to deal more broadly with the description of any material, not only mineral). Two types of cutting were evidenced in the gemstone: flat and cabochon. Flat polished plates represent the first type on both sides; the colour is red with a very fine brownish tint. The second type is red stones, cut into tall round cabochons, with the colour of these stones being more blood red with a subtle cinnamon shade. There are three bluish-green inlays on the front as well. Each of the measured stones in this buckle was assigned a unique number, under which it appeared throughout the analytical work. All found objects are now part of the archaeological collection of the T. G. M. Rakovník Museum and can be found in the inventory under No. A 2964 a, b. The analyses were performed with maximum regard to sample dimensions.

Optical microscopy and photography

Colour, transparency, and lustre were observed in a macroscopic way with Carl Zeiss's Binocular Microscope. Gemstone close-up photographs (Fig. 4) of the surface of the garnets were obtained with the Olympus BX41 microscope using LabSpec 6 software.

Optical microscopy of the filler was performed in Gemmological Laboratory Prague, using a binocular magnifier (Leica A60 Microscope with a VESA mount) at a magnification of 7–120× in incident ring light illumination (5500 K and 3500 K) and ultraviolet light at wavelengths of 254, 365 and 405 nm.

FT-IR spectroscopy

An attempt was made to confirm or refute the detection of C–H bonds in the studied samples taken from damaged parts of the gold catch plate (in search of any organic matter such as pitch, glue, etc.). The filler was scanned using attenuated total reflection-Fourier transform infrared (ATR-FTIR) spectrometer to obtain high-resolution mid-IR and far-IR spectra showing the presence of organic substances. The ALPHA II FTIR spectrometer was used for this analysis, with the region of interest set from 4000 cm^{-1} to 450 cm^{-1}.

Micro-Raman spectroscopy

Micro-Raman spectroscopy was used to identify the contained minerals and other phases. Raman spectra of all samples were obtained at room temperature at the Department of Geological Sciences, Masaryk University, Czech Republic, with a Horiba LabRAM HR Evolution (Horiba Jobin–Yvon) Raman spectrometer system equipped with a Peltier-cooled CCD detector and coupled to an Olympus BX41 microscope. Raman spectra were calibrated using the Rayleigh line. For analysis, lasers of different wavelengths were used: 532 nm (green) and 633 nm (red) to capture possible luminescence and eliminate certain inconsistencies. Data were collected in the 100–2000 cm^{-1} range using a diffraction grating with 1800 grooves/mm, an entrance slit of 100 µm, a confocal hole of 300 µm and a 50 × long-working-distance objective. Acquisition time was set to 40 s, and two accumulations were to mediate fast and high-quality measurements of the volume of the studied stones. Data were processed with SeaSolve PeakFit 4.1.12, Spectragryph 1.2.16 software and LabSpec 6 software.

UV–VIS-NIR spectroscopy

Optical absorption spectra were measured on a GL Gem Spectrometer with Toshiba TCD1304DG linear array detector (3648 Pixel size). Data were obtained from 300 to 1000 nm (optimised for

VIS–NIR—400–950 nm range). The signal-to-noise ratio was improved by fast onboard averaging and diffraction order sorting filter to eliminate second-order effects. The spot diameter on the sample was between 3 and 4 mm. Light was focused on the surface of a tall round cabochon, where the transmitted light could be collected and transferred through the SMA 905 optical fibre to the spectrometer. Flat polished cuts were not measured. Spectra were processed with "Point & Shoot" software (version 3.4).

X-ray computed tomography

For CT purposes, an XT H 450 2D/2D tomography device from Nikon Metrology was used, which is equipped with a line X-ray detector. It is a tomographic device housed in a fully shielded and automatically blocked X-ray cabinet. The device uses a rotary scanning system; it is equipped with a four-axis programmable manipulator for setting the position of the studied objects in the process of self-scanning. The primary technical data of the used tomographic equipment are: Maximum accelerating voltage and power of the reflective X-ray source was 450 kV, the focus size of the X-ray source at a power of 200W is 80 µm. For X-ray sensors (16-bit resolution depth), the curved diode line detector for 2D tomography has 400 µm per pixel, totalling 2048 pixels. CT PRO 2D software from Nikon Metrology was used to reconstruct the CT volume. Visualisation and analyses of the historical artefact were performed in VG Studio MAX v. 3.3.2 software from Volume Graphics GmbH. The 3D CT method was used as well. However, 3D proved unsuitable in the analysis due to the high incidence of image defects in the CT volume data. For this reason, the 2D method was chosen, which took longer but achieved better and more precise results [28].

Results

Optical microscopy

Different material surfaces can be distinguished based on the microscopic observation in reflected light. The grinding process is different for the individual identified precious stones (Cr-pyrope, almandine) and glass (Fig. 3). The surfaces of Cr-pyropes have both thin straight scratches and strong lines of torn material, almandine plates and cabochon surfaces typically only have consecutive light scratches. Unlike garnets, which are quite chemically resistant, the glass was affected by the way the object was deposited, and there is a certain noticeable degree of chemical etching (interference colours) due to contact with humic acids. The conchoidal fracture, typical for glassy materials, can also be observed.

Optical microscopy observation of the filler between the gold framework and gemstones was found to have a dusty character with visually distinguishable tiny whitish grains (anisotropic minerals) without any crystallographic shapes. Some light and dark mica were present, as well as black opaque grains in the material. The sample also contains little scales of gold, which could have entered the filler due to manipulation during the production of jewellery (Fig. 4a).

Spectroscopic techniques

FT-IR spectroscopy was used only for the filler study. The analysis was mainly focused on the presence of C–H bonds typical in the area around 3000 cm^{-1}. Since no bands around 3000 cm^{-1} were found (respectively, its presence is below the detection limit), we could not confirm any organic matter (this also correlates with no luminescence in UV light). Its presence at the time of manufacturing is possible [29, 30]. However, its gradual degradation during the deposition of objects in the soil cannot be ruled out. The remaining bands from 1250 cm^{-1} to 450 cm^{-1} should belong to a combination of quartz and mica (Fig. 4b). The stretching and bending

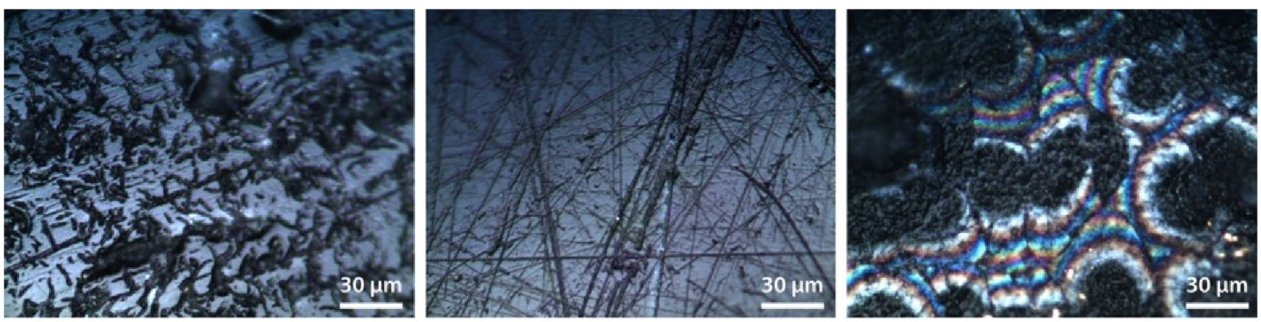

Fig. 3 Detailed photos of different surfaces of the studied stones as observed in Olympus BX41 microscope. (Photos by K. Sobek)

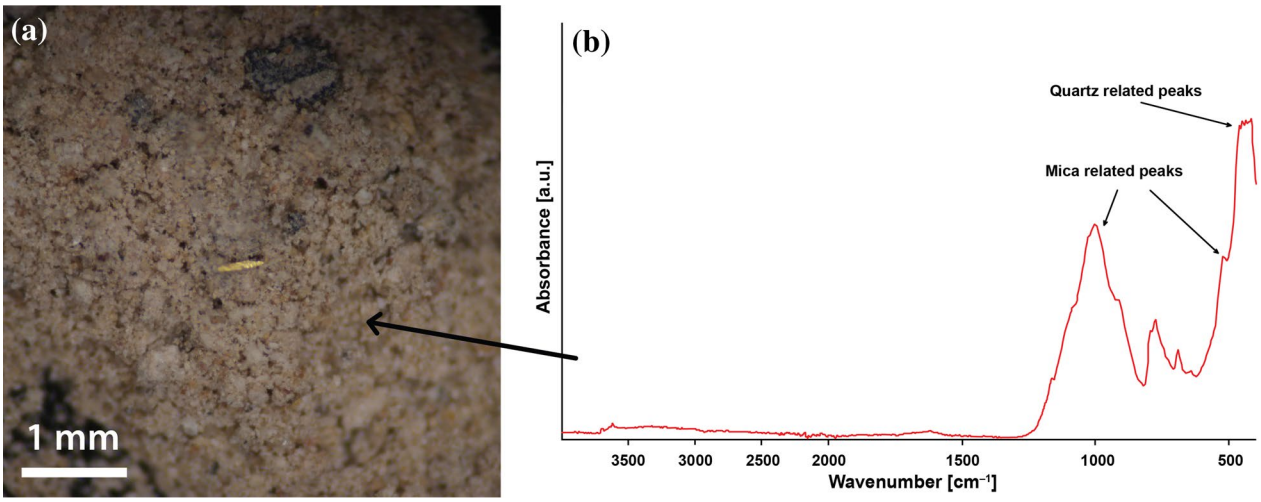

Fig. 4 Photo of a microscopic flake of gold in the filler material. Magnification ×60, incident ring light (**a**; photo by R. Hanus) and FT-IR spectrum of the marked part of the filler (**b**)

frequencies of Si–O are especially noticeable at around 1000 and 500 cm^{-1}, with dominant quartz peak at about 470 cm^{-1}.

Micro-Raman spectroscopy was used to study gemstone inlays (Fig. 5a). Yielded spectra helped to differentiate between two types of end members belonging to the supergroup of garnets. Differently shaped flat cut stones set inside the gold catch plate of a belt buckle or on the sides were identified by the spectrum as one of the garnet end members called almandine. The rounded cabochons along the edge of the top catch plate of the belt buckle were identified as pyropes. Inclusions were also detected that contaminated the Raman spectra of the garnets (inclusions were also observed under the microscope). Another examined part was the bluish-green inlays marked as S1 and S2. Raman spectroscopy confirmed that inlays are a type of glass where the measured shape of the spectrum is typical for glassy amorphous materials.

In the optical absorption spectra, it was possible to analyse only cabochon garnets around the edges. Due to the construction features of the used spectrometer, UV–VIS–NIR spectra of almandines or glass were impossible to measure. The measured optical spectra in the UV–VIS–NIR region are characterised by a significant increase in intensity, with the highest peak around 600 nm and a minor peak around 690 nm (Fig. 6).

X-ray computed tomography

The visualisation, thanks to the X-ray computed tomography of the gold framework of the belt buckle, allowed a better understanding of the placement of the gold reflective foil underneath the garnets and determined the set level and placement of the gemstone inlays. Unfortunately, tomographic data of the gemstone inlays were significantly attenuated in the obtained tomographic volumes without the possibility of their further tomographic visualisation and analysis. The location and position of the extension rivets and their mountings for attaching (six of these mountings and four rivets) were also found hidden inside the catch plate (Fig. 7).

Discussion

Gemstone inlays

Based on processing and optical microscopy, the inlays can be distinguished as three different materials. The whole process of grinding and polishing (and most likely also cutting) was done manually based on the mechanical traces observed on the surface of all the stones that were examined with no repeated pattern, which is characteristic of pro-rotation sanders or hand-circular sanding. On the contrary, the detected traces correspond to the grinding style when the polished stone moves horizontally on the grinding (polishing) mat [31].

To distinguish pyrope and almandine, we can use specific placements of individual Raman bands, which are mainly characteristic vibrations of the SiO_4 tetrahedron, its rotation, or bending and stretching due to the internal arrangement of the structure (e.g. 352 cm^{-1} and 921 cm^{-1} for almandine versus 362 cm^{-1} and 919 cm^{-1} for pyrope). In the case of the almandine spectrum, we can observe small nuances in vibrations around 350 cm^{-1} mainly because the composition of the almandine garnets can be variable, and the spectrum then corresponds to the individual ratios of the almandine component with other mineral chemistry from the pyralspite group—the silicate garnet system

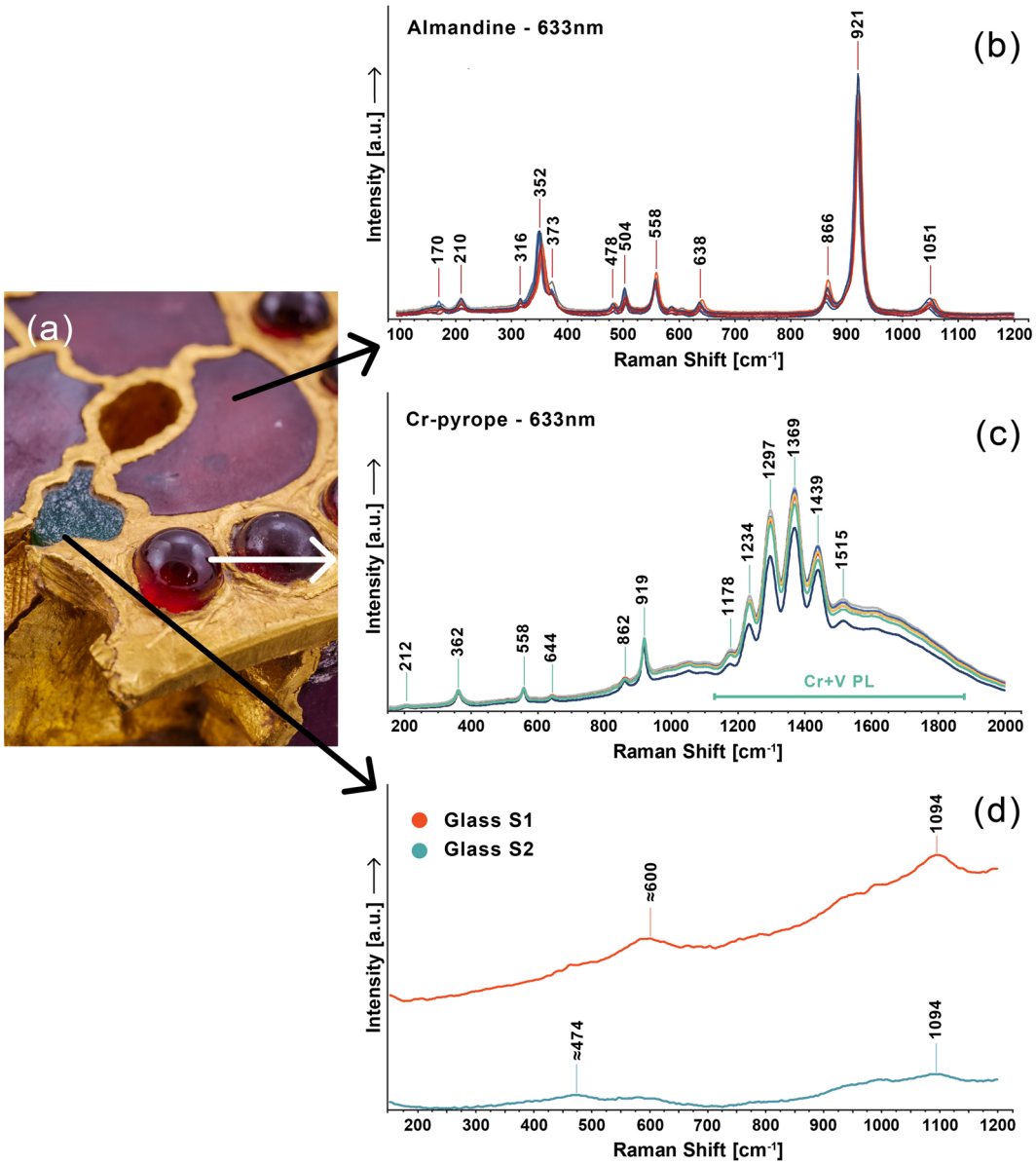

Fig. 5 Detailed photo of flat cut almandines and glass inlays in the middle of the catch plate of the belt buckle with rounded pyropes around the edges (**a**; photo by M. Frouz) and set of Raman spectra with almandine without any present luminescence (**b**); with a strong luminescence from 1200 to 1800 cm^{-1} (marked in green) typical for Cr-pyrope (**c**) and glass spectra for bluish green inlays (**d**)

pyrope–almandine–spessartine solid solution [23, 32]. Orientation during measurement can also affect the overall shape and intensity of the Raman bands in the spectrum [33]. The pyrope spectrum was also contaminated by strong photoluminescence (Fig. 5c) due to the presence of Cr (excited by a 633 nm laser), which is characteristic of Cr-pyropes (Bohemian garnet) due to its shape and intensity of bands [34, 35]. This feature was not present in almandines (Fig. 5b). Similar luminescence values were also measured by [36], but due to the use of a green laser with a wavelength of 532 nm, they are located further from the Raman spectrum in a position around 4300 cm^{-1}. Bohemian garnet typically has a relatively high presence of chromium and a minor concentration of vanadium [19]. The small peak around 690 nm and the more intense band around 600 nm relate most probably to Cr^{3+} (Fig. 6). According to the study [37], the presence of another chromophore in the form of V^{3+} cannot be clearly demonstrated. Unfortunately, the spectra below 550 nm behave atypically [46];

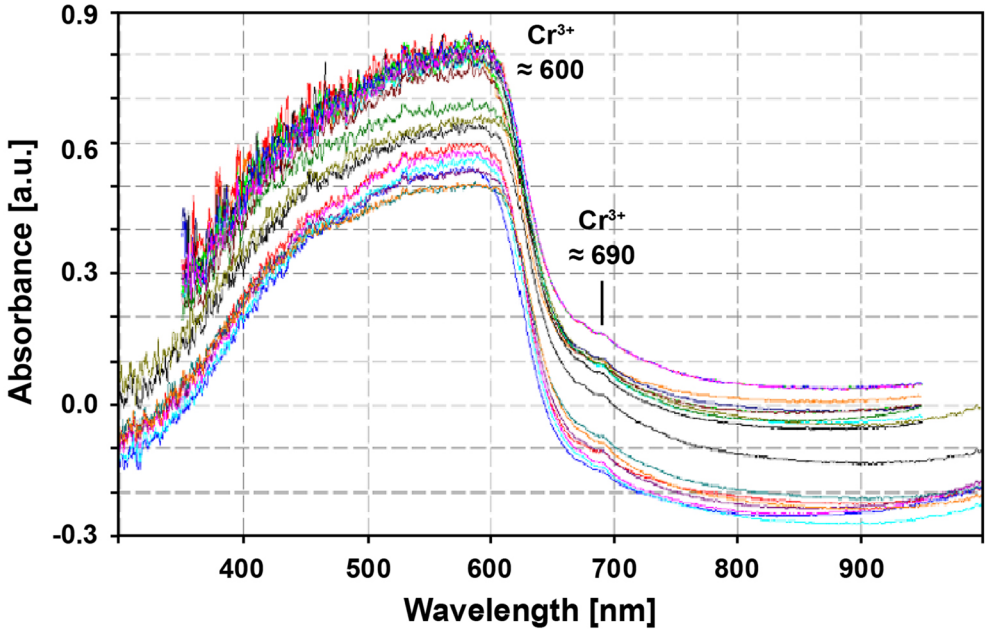

Fig. 6 Stacked absorption spectra for pyropes K1-K21 showing significant intensity in the region around 600 nm, indicating chromium presence

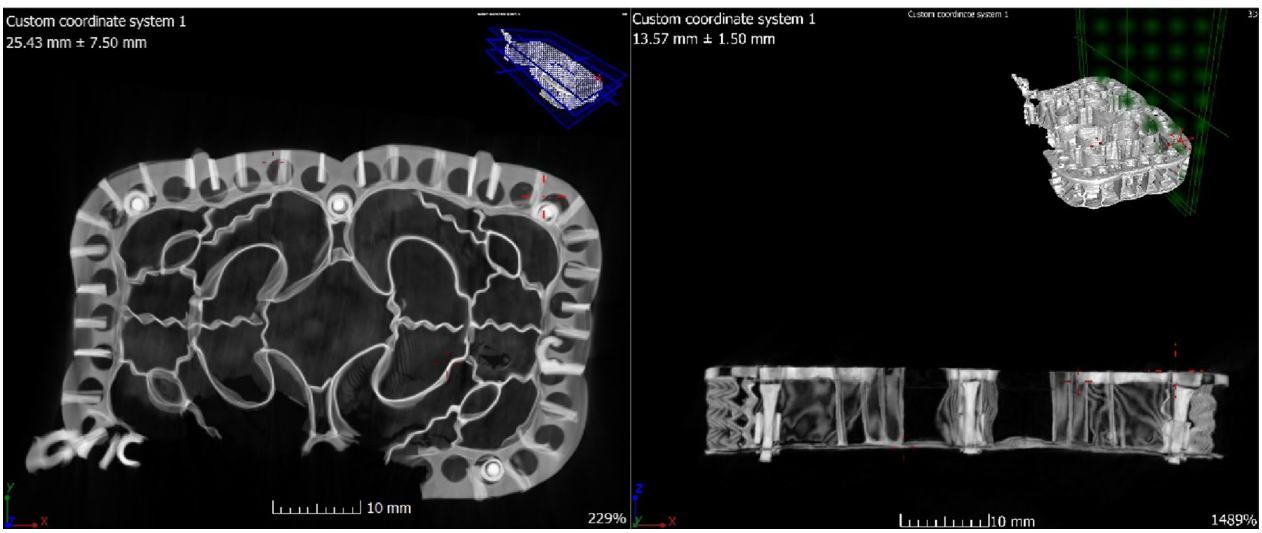

Fig. 7 Visualisation of projected 2D tomographic sections in the perpendicular plane "YX" (left) and the horizontal plane "ZX" (right) showing the location of the sliding rivets within the mountings

this may indicate some other admixture or the effect of contamination by artefacts during the complicated measurement.

Raman spectra yielded in glass inlays correlate with the possible band positions for soda-lime glasses of that age [38]. A roughly 5000 cm^{-1} strong luminescence was recorded, which most likely belongs to a type of chromophore or decolouring compound present in the glass structure [39]. The spectrum similarity for the lower spectrum (S1) can also be interpolated with the characterisation of blue glass by [40], the spectra of which correspond well to smalt (Co glass). The upper spectrum (S1) is similar to green glass in [41], which refers to some Fe impurities.

Data obtained from measurements across many studies on similar pieces of jewellery [7, 9, 42] show considerable

agreement not only in the certain band positions but also in the form of mineral inclusions (masked mainly by a strong garnet Raman signal). Based on this data, the conditions in which these minerals were formed might be assumed [12, 42, 43]. Observed mineral inclusions—apatite, mica and rutile—are typical in almandines and might indicate specific metamorphic conditions related to amphibolite facies of medium-grade metamorphism [9]. Such rock formations can also be found in certain parts of East India or Sri Lanka [9, 16], and imports of precious red stones (garnets, spinels and others) from the Orient have been known since the Late Roman Byzantine Empire [44]. Mining of very similar precious stones is still carried out today. Thus, given the historical aspects, these sources are highly plausible. A similar principle can be applied to Bohemian garnets, where quarries still produce characteristic chromium-rich pyropes [19], the analyses of which correlate with our data.

Gold framework

Visualisation based on industrial X-ray computed tomography (CT) allows detailed examination of the object using suitably oriented 2D tomographic sections [45]. These data helped to map every part of the gold framework. The first area of interest was the position of the gold reflective foil placed under the decorative stones (Fig. 7). The depth of placement of this raster gold foil from top to bottom is approximately 1.3–1.6 mm. The overall shape and dimensions of the sliding rivets differ from piece to piece [3]. The head of the rivet has a pseudo-square cross-section with a small hollow, which in this case could have been used for riveting. This square head then further passes into the cylindrical part of the sliding mounting. Rivets are more or less symmetrically distributed around the body of the catch plate, missing only on the left edge (see Fig. 7, left middle part). From the projected sections, it is clear that the sliding rivets are well hidden behind the attachment of Bohemian garnets.

Due to the relatively high difference in the bulk density of gold (approx. 19.3 g/cm^3) in comparison to the gemstones used and the filler in the compartments of the studied item (approx. 2–4 g/cm^3), it was possible to analyse only its gold framework and other parts, such as the base foil under the gemstones or the sliding rivets with their mountings for attaching the catch plate of the buckle to some kind of leather strap or sheath. The total

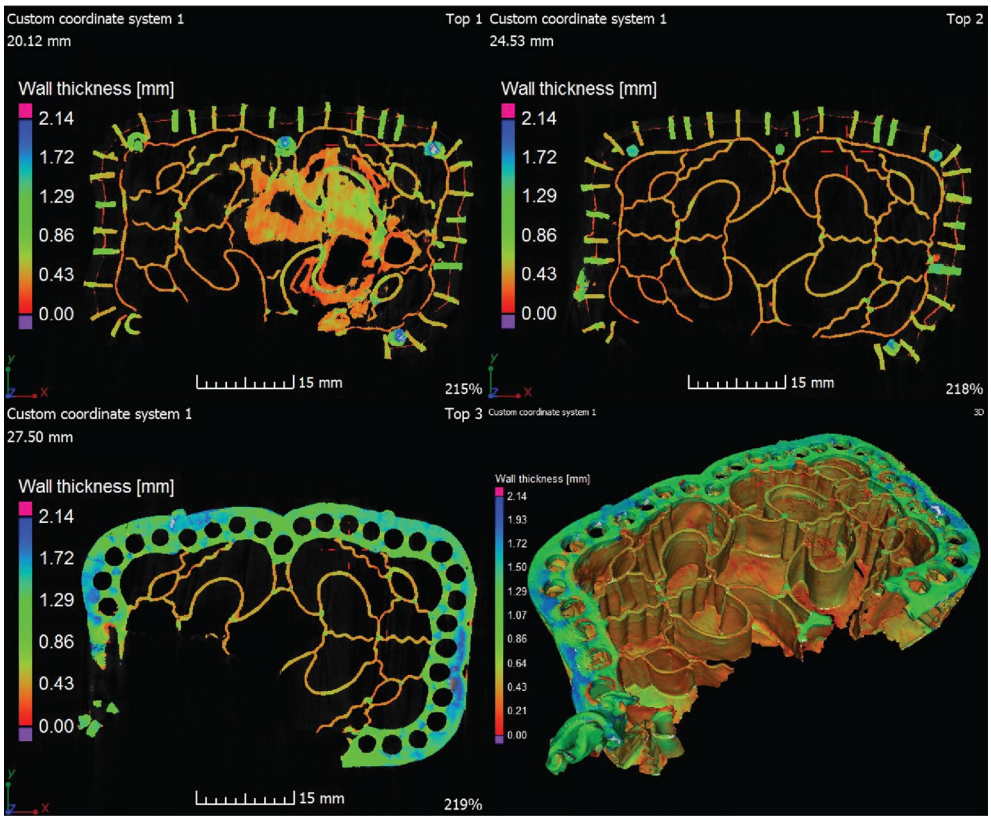

Fig. 8 Visualisation analysis of the artefact's wall thickness and the dimensions of its gold framework

volume of the gold representing the framework and its other gold parts was calculated to be around 4.2 cm^3.

The virtual image of the catch plate's frame (Fig. 8) was also extracted into an "STL" file describing the object's surface using triangulation, which characterises the surface geometry of 3D objects and is used in 3D printing. Based on this simulation, an exact 3D print model was also created [27]. This model can be used for goldsmithing purposes to make an accurate replica.

Conclusions

This paper presents new and detailed research on the gold catch plate and its gemstones using state-of-the-art analytical techniques. The obtained data has expanded our knowledge of jewellery from the Late Antique Period and contributed to a better understanding of the manufacturing technology of that age. These methodologies can be applied to jewellery and other artefacts from both the Late Antique Period and other various ages. Raman spectroscopy has proven to be a very suitable method for determining the gemstone inlays present in this belt buckle's gold catch plate. Thanks to quick and precise analysis and a suitably selected laser (633 nm), it was easy to recognise two different types of minerals from the garnet supergroup (namely the Cr-pyrope situated around the edge of the front-facing part of the catch plate and the almandine situated everywhere else) and the bluish-green inlays as a form of glass without destroying the sample. The filler underneath the gemstone inlays revealed that it had possibly been manipulated by a goldsmith; however, apart from the mineral composition, the filler could not be identified in greater detail due to the age and conditions of deposition.

X-ray computed tomography showed us a three-dimensional internal visualisation of the gold framework. Using this research method, it was possible to map visible parts, discover and investigate the hidden details of the gold catch plate of the belt buckle, analyse the wall thickness of the gold framework, or calculate the volume of gold needed for the goldsmith work. It was also possible to calculate the exact placement depth of the gold foil. X-ray computed tomography proved to be a very effective method, mainly because it helped to reveal the sliding rivets found in the internal structure of the catch plate. However, due to the complexity of the artefact, it should also be noted that the methodology of 3D tomography may not always be the most suitable; in our case, the use of 2D sections and the subsequent composition of these sections into 3D models proved to be much more effective. This three-dimensional visualisation can be processed as an exact copy constructed using 3D printing, which can be used for further research and museum purposes.

Supplementary Information

The online version contains supplementary material available at https://doi.org/10.1186/s40494-023-00874-y.

Additional file 1: Fig. S1. Comparison of Raman spectra and their luminescence between different spectra of four pyropes. The first two spectra with the most intense luminescence belong to the Bohemian garnet, where there is a match between the recently collected sample from Granátka (Czech Republic) and the artefact. The reference spectrum from Ant Hill (USA) also shows luminescence but is significantly quenched due to iron and different chromium ratio. The spectrum of garnet from Shavaryn Tsaram (Mongolia) shows no luminescence. The spectra also differ slightly due to the shifts of the vibrational bands, which are caused by the different ratios of the components of the garnet solid solution.

Acknowledgements

We would especially like to thank the management of the T. G. M. Museum in Rakovník, p.o., for allowing the study of this treasured item (stored in the archaeological collection), namely Mgr. K. Blažková and the director of the museum Mgr. Magdalena Elznicová Mikesková. At the same time, we would like to thank Dr Z. Losos and Dr R. Škoda, that allowed measurements in laboratories at the Department of Geological Sciences in Brno under strict safety conditions. We would like to thank the anonymous reviewers for their considerable contribution to this article.

Author contributions

RH: Gemmological analyses, wrote the sample description parts. Project and research management. Prepared Figs. 1, 2, 3. KSobek: Raman spectroscopy wrote the main manuscript text. Interpretation of all spectroscopic analyses. Prepared Figs. 3, 4, 5, 6 and Additional file 1. KSouček: X-ray computed tomography, data acquisition, (Figs. 7, 8). LS: X-ray computed tomography, data acquisition, 3D printing. LG: Wrote the X-ray computed tomography chapter. AS: Wrote the archaeological parts and manipulation with the artefacts. All authors read and approved the final manuscript.

Funding

The research in this article (A non-destructive analytical study of cultural heritage object from late Antiquity—gold framework and gemstone inlays) was supported by a project for the long-term conceptual development of research organisation (RVO:68145535), including the Central Bohemian regional office, the founder of the T. G. M. Museum in Rakovník and institutional support of long-term conceptual development of the research organisation Technical Museum in Brno provided by the Ministry of Culture of the Czech Republic.

Availability of data and materials

The authors confirm that the data supporting the findings of this study are available within the article and its Additional file 1. Photographs by M. Frouz (not the author) may be published with his full consent (if necessary, a written statement from him can be obtained).

Declarations

Competing interests

The authors declare that they have no known competing financial interests or personal relationships that could have appeared to influence the work reported in this paper

Received: 31 August 2022 Accepted: 27 January 2023
Published online: 16 February 2023

References

1. Horedt K, Protase D. Das Zweite Fürstengrab von Apahida (Siebenbürgen). Germania. 1972;50(1–2):174–220.

2. Niculescu G, Oanță-Marghitu R, Georgescu M (2011) In: Turbanti-Memmi I (ed.). Proceedings of the 37th International Symposium on Archaeometry (ISA 2008), Siena, Italy, 12–16 May 2008. Springer-Verlag, Berlin Heidelberg, p. 617.
3. Oanță-Marghitu R, Niculescu Gh, Şecläman D, Bugoi R, Georgescu M. (2009) ArcheoSciences-Revue d'Archeometrie 33: 227–234
4. Adams N (2011) The garnet millennium: the role of seal stones in garnet studies. In: Gems of Heaven: Recent Research on Engraved Gemstones in Late Antiquity c. ad 200–600, vol 177. British Museum, London, 10–24.
5. Bugoi R, Oanta-Marghitu R, Calligaro T. IBA investigations of loose garnets from Pietroasa, Apahida and Cluj-Someşeni treasures (5th century AD). Nucl Inst Methods Phys Res Sect B. 2015;371:401–6. https://doi.org/10.1016/j.nimb.2015.09.038.
6. Jiřík J (2021) New findings connected with the culture of elites of the Migration Period of princely nations from Mšec, Řevničov and Lipany in Central Bohemia. – Proceedings of the conference, Archeológia barbarov, Trnava, Slovakia. (in Czech, in press)
7. Calligaro T, Colinart S, Poirot JP, Sudres C. Combined external-beam PIXE and μ-Raman characterisation of garnets used in Merovingian jewellery. Nucl Inst Methods Phys Res B. 2002;189:320–7. https://doi.org/10.1016/S0168-583X(01)01078-3.
8. Horváth E, Bendő Z. Provenance study on a collection of loose garnets from a gepidic period grave in Northeast Hungary. Archeometriai Muh. 2011;8:17–32.
9. Kos S, Dolenec M, Lux J, Dolenec S. Raman Microspectroscopy of Garnets from S-Fibulae from the Archaeological Site Lajh (Slovenia). Minerals. 2020;10(4):325. https://doi.org/10.3390/min10040325.
10. Mathis F, Vrielynck O, Laclavetine K, Chêne G, Strivay D. Study of the provenance of Belgian Merovingian garnets by PIXE at IPNAS cyclotron. Nucl Instrum Methods Phys Res B. 2008;266:2348–52. https://doi.org/10.1016/j.nimb.2008.03.055.
11. Hilgner A, Greiff S, Quast D (2017) Gemstones in the First Millennium AD: mines, trade, workshops and symbolism. – Römisch Germanisches Zentralmuseum, Mainz.
12. Schönig J, Meinhold G, von Eynatten H, Lünsdorf NK. Provenance information recorded by mineral inclusions in detrital garnet. Sediment Geol. 2018;376:32–49. https://doi.org/10.1016/j.sedgeo.2018.07.009.
13. Deer WA, Howie RA, Zussman J. An Introduction to the Rock-Forming Minerals. 2nd ed. London: Longman; 1992.
14. Sibi N, Subodh G. Structural and microstructural correlations of physical properties in natural almandine-pyrope solid solution: $Al_{70}Py_{29}$. J Electr Mater. 2017;46:6947–56. https://doi.org/10.1007/s11664-017-5801-5.
15. Kataria P. Book review: geology of Rajasthan: status and perspective. J Geol Soc India. 2000;55:452–3.
16. Schmetzer K, Gilg HA, Schüssler U, Panjikar J, Calligaro T, Périn P. The linkage between garnets found in India at the Arikamedu archaeological site and their source at the Garibpet Deposit. J Gemmol. 2017;35(7):598–627. https://doi.org/10.15506/JoG.2017.35.7.598.
17. Rameshchandra PP. Mineral resources of Telangana State, India: the way forward. Int J Innov Res Sci Eng Technol. 2014;3:15450–9.
18. Jayamali MK, Bandara W, Gunatilake J, Francis P, Jayasinghe RM, Dharmasiri RM. Gem potential mapping based on Geographical Information Systems (GIS): a case study from Medagama, Moneragala District, Sri Lanka. J Geol Soc Sri Lanka. 2017;18:115–27.
19. Hanus R, Hladký P, Hyršl J, Jiránek J, Kotrlý M (2019) Gemmological definition of Bohemian garnet. – Bohemian garnet - history, identification and processing in the context of museum collections, Brno Technical Museum, Brno (in Czech)
20. Caincross B. Geology of East Africa. In minerals & gemstones of East Africa. Struik Nature: Cape Town; 2019.
21. Smith GD, Clark JHR. Raman microscopy in archaeological science. J Archaeol Sci. 2004;31:1137–60. https://doi.org/10.1016/j.jas.2004.02.008.
22. Bersani D, Andò S, Vignola P, Moltifiori G, Marino GI, Lottici PP, Diella V. Micro-Raman spectroscopy as a routine tool for garnet analysis. Spectrochimica Acta A. 2009;73(1):484–91. https://doi.org/10.1016/j.saa.2008.11.033.
23. Kolesov BA, Geiger CA. Raman spectra of silicate garnets. Phys Chem Miner. 1998;25:142–51. https://doi.org/10.1007/s002690050097.
24. Albertin F, Bettuzzi M, Brancaccio R, Morigi MP, Casali F. X-ray computed tomography in situ: an opportunity for museums and restoration laboratories. Heritage. 2019;2(3):2028–38. https://doi.org/10.3390/heritage2030122.
25. Hughes WS. CT Scanning in Archaelogy. In: Saba L, editor. Computed tomography: special applications. London: IntechOpen; 2011. p. 57–70.
26. du Plessis A, Steyn J, Roberts DE, Botha LR, Berger LR. A proof of concept demonstration of the automated laser removal of rock from a fossil using 3D X-ray tomography data. J Archaeol Sci. 2013;40(12):4607–11. https://doi.org/10.1016/j.jas.2013.07.024.
27. Franco DGDP, Camporesi C, Galeazzi F, Kallmann M. 3D printing and immersive visualisation for improved perception of ancient artifacts. Presence Teleoper Virtual Environ. 2015;24(3):243–64. https://doi.org/10.1162/PRES_a_00229.
28. Maher AM. X-RAY computed tomography of a late period falcon bronze coffin. Radiat Phys Chem. 2020;166:108475. https://doi.org/10.1016/j.radphyschem.2019.108475.
29. Arrhenius B (1985) Merovingian Garnet Jewellery. Emergence and Social Implications, Stockholm.
30. Langejans G, Aleo A, Fajardo S, Kozowyk P. Archaelogical Adhesives—Oxford Research Encyclopedia of Anthropology. Oxford: Oxford University Press; 2022. https://doi.org/10.1093/acrefore/9780190854584.013.198.
31. Klein C (2005) Faceting History: Cutting Diamonds and Colored Stones. – Xlibris Corporation, USA, p. 242
32. Geiger CA. A tale of two garnets: the role of solid solution in the development toward a modern mineralogy. Am Mineral. 2016;101:1735–49. https://doi.org/10.2138/am-2016-5522.
33. Nasdala L, Schmidt C. Applications of Raman spectroscopy in mineralogy and geochemistry. Elements. 2020;16:99–104. https://doi.org/10.2138/gselements.16.2.99.
34. Hanus R (2013) Bohemian garnet: history, geology, mineralogy, gemmology, and jewellery. Granit, Prague. (in Czech)
35. Hanus R (2019) Photoatlas of inclusions in bohemian garnet and its limitations. Prague.
36. Štubňa J, Hanus R, Malíková V (2021) New definition of the Czech (Bohemian) garnet and identification. 1. 13–20.
37. Sun Z, Palke AC, Renfro ND, Rizzo JM, Hand DB, Sanchez D. Quantitative definition of strength of chromophores in gemstones and the impact on color change in pyralspite garnets. Color Res Appl. 2022;47(5):1134–54.
38. Donais MK, Pevenage VJ, Sparks A, Redente M, George BD, Moens L, Vincze L, Vandenabeele P. Characterisation of Roman glass tesserae from the Coriglia excavation site (Italy) via energy-dispersive X-ray fluorescence spectrometry and Raman spectroscopy. Appl Phys A. 2016;122(12):1050. https://doi.org/10.1007/s00339-016-0566-x.
39. Croveri P, Fragala I, Ciliberto E. Analysis of glass tesserae from the mosaics of the "Villa del Casale" near Piazza Armerina (Enna, Italy). Chemical composition, state of preservation and production technology. Appl Phys A. 2010;100:927. https://doi.org/10.1007/s00339-010-5670.
40. Robinet L, Neff D (2008) Raman spectrometry, a non-destructive solution to the study of glass and its alteration. In ICOM Committee for Conservation 15th triennial meeting.
41. Baert K, Meulebroeck W, Ceglia A, Wouters H, Cosyns P, Nys K, Thienpont H, Terryn H (2012) The potential of Raman spectroscopy in glass studies. In Integrated Approaches to the Study of Historical Glass, 8422, 54–62. SPIE. doi: https://doi.org/10.1117/12.981648
42. Périn P, Calligaro T, Vallet F, Poirot PJ, Bagault D (2007) Provenancing Merovingian garnets by PIXE and μ-Raman spectrometry. In: Henning J (ed.), Post-Roman Towns, Trade and Settlement in Europe and Byzantium 1, Berlin, 69–76.
43. Zack T, von Eynatten H, Kronz A. Rutile geochemistry and its potential use in quantitative provenance studies. Sediment Geol. 2004;171:37–58. https://doi.org/10.1016/j.sedgeo.2004.05.009.
44. Farges F. Mineralogy of the Louvres Merovingian garnet cloisonné jewelry: origins of the gems of the first kings of France. Am Miner. 1998;83:323–30.
45. Kak AC, Slaney M (1988) Principles of computerised tomographic imaging. The Institute of Electric and Electronics Engineers Inc, IEEE Press, New York.

46. Sun Z, Palke A, Renfro N. Vanadium- and chromium-bearing pink pyrope garnet: characterisation and quantitative colorimetric analysis. Gems Gemmol. 2016;51(4):348–69. https://doi.org/10.5741/GEMS.51.4.348.

Publisher's Note